Monojet plus soft dilepton signal from light higgsino pair production at LHC14

Howard Baer, Azar Mustafayev, and Xerxes Tata

Monojet plus soft dilepton signal
from light higgsino pair production at LHC14

Howard Baer[1,2*], Azar Mustafayev[3†] and Xerxes Tata[3§]

[1]*Dept. of Physics and Astronomy, University of Oklahoma, Norman, OK 73019, USA*
[2]*William I. Fine Theoretical Physics Institute, University of Minnesota, Minneapolis MN 55455, USA*
[3]*Dept. of Physics and Astronomy, University of Hawaii, Honolulu, HI 96822, USA*

Abstract

Naturalness arguments imply the existence of higgsinos lighter than 200-300 GeV. However, because these higgsinos are nearly mass degenerate, they release very little visible energy in their decays, and (even putting aside triggering issues) signals from electroweak higgsino pair production typically remain buried under Standard Model backgrounds. Prospects for detecting higgsino pair production via events with monojets or monophotons from initial state radiation are also bleak because of signal-to-background rates typically at the 1% level. Here, we consider the possibility of reducing backgrounds by requiring the presence of soft daughter leptons from higgsino decays in monojet events. We find that LHC14 experiments with an integrated luminosity of 300 fb^{-1} should be sensitive to light higgsinos at the 5σ level for $\mu < 170$ GeV with a $S/B \sim 8.5\%$. For an integrated luminosity of 1000 fb^{-1} (which should be possible at a high luminosity LHC) the corresponding sensitivity to μ extends to over 200 GeV though the systematic uncertainty would have to be controlled to considerably better than 5%. The corresponding reach from measurements of the rate asymmetry between monojet events with same flavour vs. opposite flavour dileptons is $\sim$10-15 GeV smaller, but does not suffer the systematic uncertainty from the normalization of the background.

*Email: baer@nhn.ou.edu
†Email: azar@phys.hawaii.edu
§Email: tata@phys.hawaii.edu

1 Introduction

The lack of super-partner signals from new physics searches at LHC8 [1, 2] (the LHC with $\sqrt{s} = 8$ TeV), together with the measured value of the mass of a Standard Model (SM)-like Higgs boson [3, 4], has led many authors to question whether weak scale supersymmetry (SUSY) as realized by the Minimal Supersymmetric Standard Model is natural: *i.e.* whether the weak scale exemplified by the values of M_Z or m_h can be obtained without large fine-tuning of model parameters. The relative insensitivity of weak scale physics to physics at very high scales (such as *e.g.* the unification scale M_{GUT} in SUSY Grand Unified Theories) was for many years (and remains) one of the driving motivations for weak scale SUSY. We stress that weak scale SUSY theories do not suffer from the huge fine-tuning problem of the Standard Model (SM): while fine-tuning in the SM is a part in 10^{26}, fine-tuning in weak scale SUSY theories, by any of several measures discussed in the literature, is typically no more than a part in $\mathcal{O}(10^4)$, and often significantly smaller [5, 6].

The well-known relation [7],

$$\frac{M_Z^2}{2} = \frac{m_{H_d}^2 + \Sigma_d^d - (m_{H_u}^2 + \Sigma_u^u)\tan^2\beta}{\tan^2\beta - 1} - \mu^2 \tag{1}$$

obtained from the minimization of the (renormalization group improved) one-loop electroweak scalar potential of the Minimal Supersymmetric Standard Model (MSSM) enables us to define Δ_{EW}, which measures the degree of cancellation between various contributions (defined at the weak scale) to obtain the measured value of M_Z^2. In (1), Σ_u^u and Σ_d^d are radiative corrections which depend strongly on the value of third generation squark masses. Expressions for the Σ_u^u and Σ_d^d are given in the Appendix of Ref. [8]. The electroweak fine-tuning parameter Δ_{EW} is defined by [9, 8, 10],

$$\Delta_{\mathrm{EW}} \equiv max_i \left|C_i\right| / (M_Z^2/2) \,, \tag{2}$$

where $C_{H_d} = m_{H_d}^2/(\tan^2\beta - 1)$, $C_{H_u} = -m_{H_u}^2 \tan^2\beta/(\tan^2\beta - 1)$ and $C_\mu = -\mu^2$. Also, $C_{\Sigma_u^u(k)} = -\Sigma_u^u(k)\tan^2\beta/(\tan^2\beta - 1)$ and $C_{\Sigma_d^d(k)} = \Sigma_d^d(k)/(\tan^2\beta - 1)$, where k labels the various loop contributions included in Eq. (1). Requiring weak scale fine-tuning smaller than $\Delta_{\mathrm{EW}}^{-1}$ then implies that,

$$|\mu|^2 < \Delta_{\mathrm{EW}}\frac{M_Z^2}{2} \,, \tag{3}$$

implying that higgsinos cannot be very heavy [11].[1]

We emphasize that the existence of light higgsinos, $\widetilde{Z}_{1,2}$ and $\widetilde{W}_1^\pm$, is a very robust feature of SUSY models with low fine-tuning. Even with other measures of fine-tuning in the literature – such as Δ_{HS} which includes the effects of large logarithms from renormalization that occur in models defined at a high scale [12, 13, 14] or the traditional measure Δ_{BG} [15, 16] which most readily incorporates correlations between weak scale parameters – light higgsinos are a must. This is often hidden because proponents of these measures often emphasize the contribution of top squark masses to fine-tuning, and the role of higgsinos is obscured. It has been noted, however, that correlations among model parameters (such as $A_0 \simeq -1.6m_0$, $m_{1/2} = (0.15 -$

---

[1]We have tacitly assumed that higgsinos obtain their mass from the superpotential μ term that then also enters the scalar Higgs potential. This is the case in all models we know of.

$0.25)m_0$, *etc.*) can lead to low Δ_{EW} along with $\Delta_{\mathrm{BG}} \simeq \Delta_{\mathrm{EW}}$ [17, 6] even for TeV scale top-squarks well beyond the LHC reach: see also Ref. [18]. Since the μ-parameter occurs directly in (1) and renormalizes relatively little between the high scale and the weak scale, models with large $|\mu|$ are necessarily fine-tuned in any theory where the super-potential parameters and the soft-SUSY breaking parameters have independent origins. For this reason, we view light higgsinos as an essential feature of SUSY models with low fine-tuning [8].

In most high scale models where parameters are defined at a scale $Q \sim M_{\mathrm{GUT}} - M_{\mathrm{Planck}}$, the Higgs soft mass is typically driven via renormalization group evolution to large (TeV-scale) negative values at the weak scale. The value of μ is adjusted (tuned) to gain the measured value of M_Z via the electroweak symmetry breaking constraint (1). As a result, in most models with relatively heavy sparticles Δ_{EW} is typically large [6]. To obtain a low values of Δ_{EW}, however, we need $m_{H_u}^2$ to be driven through zero to a value close to $-M_Z^2$ at the weak scale. Then, for moderate to large values of $\tan\beta$, we see from (1) that μ^2 will also be close to M_Z^2. A number of mechanisms have been suggested to ensure this. Perhaps the best known example occurs in the hyperbolic branch/focus point (HB/FP) region [11, 19] within mSUGRA or its extension to include non-universal third generation matter scalar masses and A-parameters [20]. Non-universality of soft-SUSY-breaking parameters in the Higgs sector also allows for low values of μ^2 [21, 22]. For instance, allowing independent choices for GUT scale Higgs mass squared parameters guarantees that one can adjust the high scale value of $m_{H_u}^2$ so that it runs down to a value not far from $-M_Z^2$ at the weak scale. Indeed, this is the idea underlying the radiatively-driven natural SUSY (RNS) framework (described in Sec. 2) that we adopt for our analysis. Low values of μ^2 can also be obtained by allowing non-universality in the gaugino sector. Models with high values of the GUT scale wino mass parameter [23] or low values of the gluino mass parameter [24] that lead to relatively low values of $|\mu|$ have been suggested in the context of well-tempered WIMPs. In a recent study [25], Martin has suggested a model where the SUSY breaking F-term also breaks the GUT symmetry via a field that is a linear combination of a **1** and **24** dimensional representation of $SU(5)$ leading to a non-universal pattern of GUT scale gaugino mass parameters [7] that results in a relatively small magnitude of μ.

At this point one may well wonder how the little hierarchy between the magnitude of μ (required to obtain low values of Δ_{EW}) and the sparticle mass scale (typified by the gravitino mass $m_{3/2}$ in gravity-mediation) arises in the first place: $\mu \ll m_{3/2}$. The answer lies in the proposed solutions to the well-known μ-problem: why is the magnitude of the supersymmetric μ term so much smaller than the Planck scale? These solutions all involve first forbidding the appearance of μ via some unspecified (perhaps Peccei-Quinn) symmetry, and then generating it via superpotential couplings to additional visible sector fields (as in the NMSSM [26]) or via non-renormalizable interactions with hidden sector fields in either the Kähler potential (Giudice-Masiero or GM) [27] or the superpotential (Kim-Nilles or KN) [28]. In GM, then one expects in gravity mediation that $\mu \sim \lambda m_{\mathrm{hidden}}^2/M_P \sim \lambda m_{3/2}$ where λ is a dimensionless coupling constant, while in KN then one expects $\mu \sim \kappa f_a^2/M_P$ where f_a is the Peccei-Quinn (PQ) symmetry breaking scale. In the former case, the little hierarchy $\mu \ll m_{3/2}$ could result from small $\lambda \sim 0.01 - 0.1$, while in the latter case it might be a reflection of a mis-match between PQ and hidden sector mass scales $f_a \ll m_{\mathrm{hidden}}$ [6].

Light higgsinos can be definitively searched for at electron-positron colliders provided that

$\sqrt{s} > 2m(\text{higgsino})$. It has been shown that at the proposed International Linear Collider (ILC) with 80% polarized electron beams – in addition to discovery – detailed measurements that unequivocally point to the higgsino origin of the signal should be possible [29] even in the very challenging case where the visible energy release in higgsino decay is as small as 10 GeV.[2] An ILC operating at $\sqrt{s} \simeq 600$ GeV should be able either to discover light higgsinos or decisively exclude the idea of natural SUSY with better than 3% EW fine-tuning, if gaugino mass unification is assumed.

In view of the importance of naturalness, it is critical to examine prospects for light higgsino discovery at the LHC where the light higgsino states $\widetilde{W}_1^{\pm}$ and $\widetilde{Z}_{1,2}$ can be pair produced by quark anti-quark collisions via the processes, $pp \to \widetilde{Z}_i \widetilde{Z}_j + X$, $pp \to \widetilde{W}_1 \widetilde{Z}_i + X$ and $pp \to \widetilde{W}_1^+ \widetilde{W}_1^- + X$ $(i, j = 1, 2)$. The produced charginos and neutralinos then decay via $\widetilde{W}_1 \to f \bar{f}' \widetilde{Z}_1$ and $\widetilde{Z}_2 \to f \bar{f} \widetilde{Z}_1$, where f and f' are SM quarks and leptons, potentially resulting in various multi-jet plus multi-lepton signatures, including the much celebrated clean trilepton signature for SUSY. The problem, of course, is that in natural SUSY where $|\mu| \ll |M_{1,2}|$ the higgsinos states all have a mass close to $|\mu|$, because the mass gaps $m_{\widetilde{W}_1} - m_{\widetilde{Z}_1}$ and $m_{\widetilde{Z}_2} - m_{\widetilde{Z}_1}$ are proportional to $M_W^2/M_{1,2}$ and typically about 10-20 GeV. As a result, the visible daughter jets and leptons from charginos and neutralino decays are very soft, and likely buried under SM backgrounds [31, 32]. The lack of a trigger for these soft events is an additional complication.

This led various groups to consider LHC prospects for discovering light higgsinos produced in association with a hard QCD jet [33, 34, 31, 35, 36, 37, 38], a photon [34, 36, 39, 40, 41, 42], W or Z boson [43, 44] or even a Higgs boson [45], where the associated particle could serve as a trigger for the event, resulting in characteristic mono-something events with nothing other than the very soft debris from $\widetilde{W}_1$ or $\widetilde{Z}_2$ decays.[3] We are pessimistic about prospects for LHC discovery of higgsino pairs via detection of monojets or mono-photons. The problem is that although a statistically significant signal might be possible, the signal to background ratio is $\sim 1\%$, *without any discernable difference in the shapes of any distributions that characterize the jet or the photon* [36, 35, 37]. We find it difficult to imagine that the absolute rates for tails of QCD backgrounds will be known to better than a percent precision required to unequivocally discover the signal.

It had been suggested [31] that LHC detection prospects of nearly mass degenerate higgsinos may be improved by requiring additional soft leptons in events. In a recent paper, Han, Kribs, Martin and Menon [47] have studied this possibility in the two-lepton plus jet channel. Motivated by the importance of the issue of naturalness, we felt that an independent examination of this topic was warranted. While we broadly agree with the conclusions of Ref. [47] (that the higgsino signal may indeed be observable at LHC14 with 300-1000 fb^{-1}), our analysis differs from that of Han *et al.* in several important respects detailed in Sec. 3. In addition, we show that the signal may also be detectable via the measurement of the rate asymmetry in monojet events with same flavour dileptons and monojet events with opposite flavour dileptons. Un-

---

[2]In models with radiatively-driven naturalness, requiring $\Delta_{\text{EW}} \le 30$ (corresponding to no worse than 3% electroweak fine-tuning), the mass gap between the next-to-lightest neutralino and the lightest SUSY particle (LSP) is always larger than 10 GeV. Even smaller mass gaps below the GeV level can also be explored at ILC via a very different technique [30].

[3]The contact interaction approximation used in many analyses of the mono-something signal is inapplicable for light higgsino models; see Ref. [46].

like the signal from a cut-and-count experiment, the flavour asymmetry measurement does not suffer from the systematic uncertainty associated with the normalization of the background.

The remainder of this paper is organized as follows. In Sec. 2 we briefly outline the RNS framework that we use for our analysis, and set up the model line that we use for our study. We describe our simulation of the signal and SM backgrounds along with our analysis cuts in Sec. 3 where we also compare and contrast our calculations with those of Han *et al.* [47]. Our projections for the LHC14 reach for higgsinos assuming integrated luminosities ranging from 100-1000 fb^{-1} form the subject of Sec. 4. We conclude in Sec. 5 with a summary of our results and our outlook for discovering natural SUSY at the LHC.

2 A model line with radiatively-driven naturalness

The RNS framework provides a setting for generating MSSM spectra with Δ_{EW} in the 10-30 range. Specifically, we generate these in the framework of the NUHM2 model [22] specified by the parameter set,

$$m_0, \ m_{1/2}, \ A_0, \ \tan\beta, \ \mu, \ m_A \tag{4}$$

consisting of the familiar mSUGRA/CMSSM parameters specified at the GUT scale, augmented by the weak scale parameters μ and m_A. The ability to specify μ and m_A independently of other parameters arises from the freedom to choose the GUT scale values of the scalar Higgs soft-SUSY breaking parameters independently of the m_0, which is why the model is referred to as the non-universal Higgs mass model with two additional parameters. If we choose $A_0 \sim -(1.5-2)m_0$ then radiative corrections in (1) from top squark loop contributions $\Sigma_u^u(\tilde{t}_{1,2})$ are suppressed even for $m_{\tilde{t}_1} = 1-2$ TeV and $m_{\tilde{t}_2} \sim (2-4)m_{\tilde{t}_1}$. The large magnitude of A_0 at the same time lifts m_h to its measured value because the top-squarks are highly mixed. Then, if we adopt $|\mu| \sim 100-300$ GeV, we find Δ_{EW} in the 10-30 range as desired [9]. The RNS spectrum is characterized by [8, 48],

- light higgsino states $\widetilde{W}_1^{\pm}$ and $\widetilde{Z}_{1,2}$ in the 100-300 GeV range (the lighter the better) with a mass gap between the heavier higgsinos and $\widetilde{Z}_1$ of about $10-30$ GeV,

- well-mixed third generation squarks with TeV scale masses,

- $m_{\tilde{g}} \leq 4-5$ TeV so that gluino loop corrections do not uplift the top squark masses.

First/second generation sfermion masses can be chosen to be in the 5-30 TeV range without jeopardizing naturalness provided one of several degeneracy patterns within first/second generation sfermion multiplets is respected [49]. Although not required by naturalness, we adopt this choice because it ameliorates the SUSY flavour problem by decoupling the new physics [50], and also addresses the proton decay [51] and gravitino [52] problems (in models where gravitinos get a mass comparable to that of these scalars).

Within the RNS framework, the mass gaps between $\widetilde{W}_1/\widetilde{Z}_2$ and the higgsino-like LSP $\widetilde{Z}_1$ decrease with increasing $m_{1/2}$. The smallest value of $m_{\widetilde{Z}_2} - m_{\widetilde{Z}_1}$ consistent with $\Delta_{\mathrm{EW}} < 30$ is about 10 GeV [29]. Since LHC signals for higgsino detection become most challenging for small

values of the mass gap, we adopt a NUHM2 model line (where we vary that parameter μ which fixes the mass scale for the higgsino-like states)

$$m_0 = 5 \text{ TeV}, \ m_{1/2} = 1 \text{ TeV}, \ \tan\beta = 15, \ A_0 = -1.6m_0, \ m_A = 1 \text{ TeV} , \qquad (5)$$

which yields $m_{\widetilde{Z}_2} - m_{\widetilde{Z}_1}$ close to 10 GeV for our initial analysis. (For completeness, we note that the lighter chargino mass tracks the $\widetilde{Z}_2$ mass and that $|m_{\widetilde{Z}_2} - m_{\widetilde{W}_1}| < 2$ GeV for 100 GeV $< \mu < 250$ GeV which, as we will see below, covers the higgsino mass range accessible at even the high luminosity LHC.) For the calculation of sparticle mass spectra and sparticle decay patterns we use the ISAJET 7.84 program [53] where we fix $m_t = 173.2$ GeV. Squarks and gluinos are very heavy ($m_{\tilde{g}} \sim 2.4$ TeV and $m_{\tilde{q}} \sim 5$ TeV) and so beyond the range of LHC14, except perhaps for ultra high integrated luminosities.

In Fig. 1, we show cross sections along this model line at a pp collider with $\sqrt{s} = 14$ TeV for the pair production of higgsino states in association with exactly one jet with $p_T > 100$ GeV jet and $|\eta_j| < 2.5$ from QCD radiation. The details of our calculation are described in Sec. 3.1. We show results for $pp \to \widetilde{W}_1^+\widetilde{W}_1^- j$, $\widetilde{W}_1\widetilde{Z}_{1,2}j$ and $pp \to \widetilde{Z}_1\widetilde{Z}_2 j$, $\widetilde{Z}_2\widetilde{Z}_2 j$ processes, for which soft leptons from subsequent decays $\widetilde{W}_1 \to \ell\nu\widetilde{Z}_1$ and $\widetilde{Z}_2 \to \ell^+\ell^-\widetilde{Z}_1$ could serve to reduce the background. We see that the cross-sections for the production of *unlike* higgsino-like states (which occurs via essentially unsuppressed electroweak couplings) in association with a jet range from $\mathcal{O}(10-100)$ fb for $\mu = 100 - 250$ GeV. In contrast, the cross section for $\widetilde{Z}_2\widetilde{Z}_2 j$ production (and also for $\widetilde{Z}_1\widetilde{Z}_1 j$ production, not shown because it gives monojet events without any additional leptons) is strongly suppressed. This is because for $|\mu| \ll |M_{1,2}|$, the lighter neutralinos are dominantly the higgsinos $(\tilde{h}_u \pm \tilde{h}_d)/\sqrt{2}$, causing the $Z\bar{\widetilde{Z}}_i\widetilde{Z}_i$ coupling to be strongly suppressed [7].

Since squarks and sleptons are very heavy, the $\widetilde{W}_1/\widetilde{Z}_2$ decay amplitudes are dominated by virtual W/Z exchange so that the leptonic branching fractions are essentially governed by W or Z boson couplings to quarks and leptons: 11% (per lepton family) for charginos, and 4% for neutralinos for the entire range of μ shown in the figure.[4] The $\widetilde{W}_1\widetilde{Z}_2 j$, $\widetilde{Z}_1\widetilde{Z}_2 j$ processes, followed by the leptonic decays of $\widetilde{Z}_2$, yield hard monojet plus soft dilepton plus E_T^{miss} events with a cross section $\sim (10-100)$ fb $\times 8\%$, corresponding to $\sim 100 - 1000$ events with this topology (before lepton acceptance cuts) per 100 fb^{-1} in the upcoming runs of LHC14. These dileptons necessarily have opposite-sign (OS) but same-flavour (SF) and their invariant mass is bounded from above by the mass gap $m_{\widetilde{Z}_2} - m_{\widetilde{Z}_1} \simeq 10$ GeV along this model-line. $\widetilde{W}_1^+\widetilde{W}_1^- j$ production can also lead to dilepton plus hard monojet events at comparable rates. In this case, however, we expect e^+e^-, $\mu^+\mu^-$ as well as $e^+\mu^-$ and μ^+e^- pairs at roughly the same rate. Though the dilepton mass is not kinematically bounded as for dileptons from $\widetilde{Z}_2$ decays, we nevertheless expect relatively low dilepton masses simply because the leptons are expected to be soft. While the signal occurs at an observable rate, there are numerous sources of SM backgrounds under which this signal can hide. These include, $(Z/\gamma^* \to \tau\bar{\tau}) + j$, $t\bar{t}$, $W^+W^- j$ discussed in Ref. [47], together with backgrounds from $(Z \to \nu\bar{\nu}) + (Z/\gamma^* \to \ell\bar{\ell}/\tau\bar{\tau}) + j$,

---

[4]The reader should keep in mind that because $m_{\widetilde{Z}_2} - m_{\widetilde{Z}_1} = 10$ GeV, $\widetilde{Z}_2 \to b\bar{b}\widetilde{Z}_1$ decays are essentially forbidden, while decays to charm and tau fermions are kinematically suppressed, causing the leptonic branching fraction to be somewhat enhanced relative to that of the on-shell Z boson.
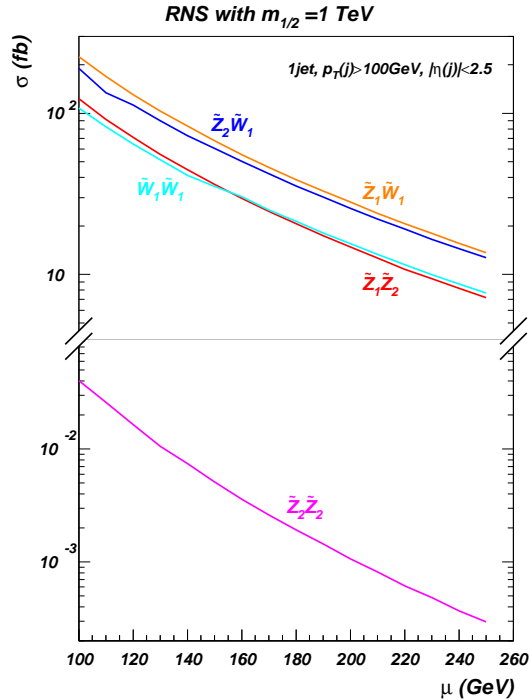
Figure 1: The production cross-sections for higgsino-like chargino/neutralino pair plus one central jet with $p_T(j) > 100$ GeV as function of μ for the RNS model introduced in (5) of the text. Notice the break in the vertical scale.

$(W \to \ell/\tau + \nu) + (Z/\gamma^* \to \ell\bar{\ell}/\tau\bar{\tau}) + j$, $(Z \to \nu\bar{\nu}) + b\bar{b} + jets$ (where leptons from the decays of b are accidentally isolated) and single top backgrounds from inclusive tW and tq' production. Note that backgrounds from $(Z/\gamma^* \to \ell\bar{\ell}) + j$ events can be efficiently removed by a E_T^{miss} cut.

Before closing this section, we note that $\widetilde{W}_1\widetilde{Z}_1$ production can give rise to single lepton plus monojet events. We expect that these will be obscured by enormous Wj and possibly top backgrounds (see also Ref. [31]) and do not consider these any further. $\widetilde{Z}_2\widetilde{W}_1 j$ production potentially yields soft trilepton plus hard monojet events. After folding in leptonic branching fractions, the total signal rate, before acceptance cuts for leptons, is just 20-200 events per 100 fb^{-1}. However, since the signal leptons tend to be very soft, we expect that the signal is severely rate limited and likely unobservable except perhaps for the smallest values of μ at the high luminosity LHC. For these reasons, the dilepton plus monojet signal will be our focus in the remainder of this paper.

3 Calculational Details

3.1 Simulation

For the simulation of the signal, we use Madgraph 5 [54] to generate $pp \to \widetilde{W}_1^+\widetilde{W}_1^-$, $\widetilde{Z}_{1,2}\widetilde{Z}_{1,2}$ and $\widetilde{W}_1^\pm\widetilde{Z}_{1,2}$ plus one-parton processes (exclusive) and plus two-partons (inclusive) where, to

increase efficiency, we require the hardest final state parton to have $p_T(\text{parton}) > 80$ GeV; the final cross section is then the sum of 1-jet exclusive and 2-jet inclusive processes. To avoid double-counting, we used the MLM scheme [55] for jet-parton matching. The events are then passed to Pythia v6.4 [56] for showering, hadronization and underlying event. We use CTEQ6L1 parton distribution functions [57] for our calculations. For the computation of the backgrounds we also use a similar procedure, except that for backgrounds with an extra jet in the final state, e.g. $\tau\bar{\tau}j$, we only generate events with exactly one parton jet, again with $p_T > 80$ GeV.

These Madgraph/Pythia events are then passed to the Isajet toy detector simulation [53] with calorimeter cell size $\Delta\eta \times \Delta\phi = 0.05 \times 0.05$ and $-5 < \eta < 5$. The HCAL (hadronic calorimetry) energy resolution is taken to be $80\%/\sqrt{E} \oplus 3\%$ for $|\eta| < 2.6$ and FCAL (forward calorimetry) is $100\%/\sqrt{E} \oplus 5\%$ for $|\eta| > 2.6$, where $\oplus$ denotes combination in quadrature. The ECAL (electromagnetic calorimetry) energy resolution is assumed to be $3\%/\sqrt{E} \oplus 0.5\%$. We use the cone-type Isajet jet-finding algorithm [53] to group the hadronic final states into jets. Jets and isolated leptons are defined as follows:

- Jets are hadronic clusters with $|\eta| < 3.0$, $R \equiv \sqrt{\Delta\eta^2 + \Delta\phi^2} \leq 0.4$ and $E_T > 40$ GeV.

- Electrons and muons are considered isolated if they have $|\eta| < 2.5$, $p_T(l) > 5$ GeV with visible activity within a cone of $\Delta R < 0.2$ about the lepton direction, $\Sigma E_T^{cells} < \min(|p_T(\ell)|/10, 5 \text{ GeV})$.

- We identify hadronic clusters as b-jets if they contain a B hadron with $E_T(B) > 15$ GeV, $\eta(B) < 3$ and $\Delta R(B, jet) < 0.5$. We assume a tagging efficiency of 60% and light quark and gluon jets can be mis-tagged as a b-jet with a probability $1/150$ for $E_T \leq 100$ GeV, $1/50$ for $E_T \geq 250$ GeV, with a linear interpolation for intermediate E_T values.

3.2 Backgrounds

We have evaluated backgrounds to the monojet plus (soft) dilepton plus E_T^{miss} signal from various SM origins:

1. $(Z/\gamma^* \to \tau\bar{\tau}) + j \to \ell^+\ell'^- j + E_T^{\text{miss}}$, whose squared matrix element we evaluate as a $2 \to 3$ process, and the taus are decayed in Pythia using the TAUOLA code [58];

2. $t\bar{t}$, where leptons come from decays of W and b quarks;

3. $W^+W^- j \to \ell^+\ell'^- j + E_T^{\text{miss}}$;

4. $(Z \to \nu\bar{\nu}) + (Z/\gamma^* \to \ell^+\ell^-) + j \to \ell^+\ell^- j + E_T^{\text{miss}}$;

5. single-top processes $bg \to tW$ and $bq \to tq'$, where the leptons come from the W and b daughters of top decay;

6. $(Z \to \nu\bar{\nu}) + b\bar{b} + jets$, where both leptons comes from the decays of the b quarks.

7. $(W \to \ell/\tau + \nu) + (Z/\gamma^* \to \ell\bar{\ell}/\tau\bar{\tau}) + j \to \ell\ell\ell' j + E_T^{\text{miss}}$.

	$\tau\bar{\tau}j$	$t\bar{t}$	WWj	$Z\gamma^*j$	$W\gamma^*j$	tW	tq	Signal
before cuts	20660	953600	460.53	5.59	171.83	62330	68080	398.7
1-event level	0.011	0.0954		0.000016		0.0312	0.068	
$N_b=0$	20395	386450	455.0	5.54	169.7	37270	41550	393.2
$N_j=1$	8020.4	33470	290.9	4.24	100.2	6945	7752	236.8
$p_T(j_1) > 100$ GeV, $\|\eta(j_1)\| < 2.5$	2961	15590	162.7	1.95	58.8	2351	3646	133.7
$E_T^{\mathrm{miss}} > 100$ GeV	935.0	12950	82.28	1.54	19.16	1700	2257	120.6
$N_\ell \geq 2$	171.3	880.8	52.26	0.56	15.0	72.79	19.75	2.20
$m_{\tau\tau}^2 < 0$	26.68	354.6	22.64	0.39	6.29	30.07	9.60	1.34
OS/SF	12.80	145.9	11.33	0.39	4.03	10.94	3.61	1.19
$m_{ll} < 10$ GeV	1.35	5.24	0.27	0.19	0.51	0.34	0.34	1.15

Table 1: Cut flow for the dominant backgrounds and for the RNS model-line point with $\mu = 150$ GeV. The first row shows the cross section after the 80 GeV cut on the parton jet. The WWj, $W\gamma^*j$ and signal cross sections are evaluated by combining several channels, making it impossible to assign a 1-event level. All cross sections are in fb.

The first three of these backgrounds have also been considered in the analysis of Ref. [47]. We were led to examine backgrounds from single top production because it has a substantial cross-section: nearly 50% of top pair production [59]. We will see that it makes a sub-dominant (but non-negligible) contribution to the background after various cuts to enhance the signal are implemented.

The results of our calculations of the various backgrounds are shown in Table 1. For reference, we also include the corresponding signal cross section for the case with $\mu = 150$ GeV along the model line introduced in (5). The first row shows the total cross-section that we obtain with the requirement of an 80 GeV parton jet in all but the $t\bar{t}$ and tW production processes in the table. Also, the $t\bar{t}$ production cross section is normalized to its NNLO+NNLL value of 953.6 pb [60] which corresponds to scaling the tree-level leading order cross-section that we obtain by a factor $k = 1.72$. Since the other backgrounds are smaller than $t\bar{t}$ and many have smaller NLO corrections $\mathcal{O}(20\%)$, we did not include any k-factors for them. Although the analysis in Ref. [61] suggests that NLO corrections to the signal can be large yielding $k \sim 2.3$, which is significantly larger than $k \sim 1.4$ for higgsino production without a jet [62], we take a conservative approach and use the LO cross section for the signal in this study.

To start with, $t\bar{t}$ is by far the dominant SM process. Requiring a b-veto, together with exactly one 100 GeV jet, reduces it by two orders of magnitude, but it is still a factor 5 larger than the single top processes, and an order of magnitude larger than $\tau\bar{\tau}j$ processes. Requiring $E_T^{\mathrm{miss}} > 100$ GeV together with 2 detected leptons (e or μ) leaves $t\bar{t}$ as the dominant background to monojet + E_T^{miss} events with a pair of soft leptons. This differs qualitatively from the results in Table I of Ref. [47] where $\tau\bar{\tau}j$ yields the dominant background. While we find the $t\bar{t}$ in Table 1 to be 881 fb, the corresponding number is 28 fb in Ref. [47]. We have traced this difference to several factors.

- We use more conservative b-tagging criteria so that the b-jet veto reduces the cross section

by just 2.5 rather than 5 used by Han *et al.*

- In contrast to Ref. [47] which has included only $t \to b\ell\nu$ $(\ell = e, \mu)$ decays of both tops, we include leptons from *all decay modes* of the t-quarks. We have checked that this increases the cross-section by a factor ~ 2.25 (of which just $\sim 1/3$ comes from $W \to \tau \to \ell$ decays). Somewhat surprisingly, including semileptonic decays from the b-daughters almost doubles the rate! This is presumably partly due to combinatorial factors, and partly due to the fact that it is easier for soft leptons to be isolated.

- Ref. [47] uses the tree-level cross-section which differs by a factor of $k = 1.72$ mentioned earlier from the NNLO+NNLL cross-section that we use.

These considerations imply that we would obtain a cross-section larger by a factor $\sim 2 \times 2.25 \times 1.72 \simeq 8$ than that in Ref. [47], still not enough to to account for the discrepancy between the two calculations. To better understand this, we attempted to reproduce the numbers in Table 1 of Ref. [47] using the cuts and simulation described therein. We were able to reproduce these results for the $(W \to \ell\nu) + (W \to \ell'\nu) + j$, but are too large by about 40% for $\tau\bar{\tau}j$ and about a factor 3 for the $t\bar{t} \to \ell\nu\ell'\nu b\bar{b}$ process. We have checked that labelling hadronic clusters with $E_T > 30$ GeV as jets, as in Ref. [47], reduces the $t\bar{t}$ background by factor of 1.7. Extending the jet rapidity acceptance to $|\eta| < 4.5$ increases the reduction to 1.9, accounting for the bulk of the difference of the $t\bar{t}$ background for that in Ref. [47].

For the WWj process – in addition to both Ws decaying to ℓ that was considered in Ref. [47] – we also included channels where one or both W bosons decay to tau: $W \to \tau\nu \to \ell\nu\nu\nu$. Although here one is penalized by the leptonic branching fraction of taus, $BR(\tau \to \ell\nu\nu) \simeq 0.35$, the resulting leptons are typically soft and thus contribute to our range of interest. As a result of inclusion of $W \to \tau \to \ell$ decay chains, the WWj cross section after the $N_\ell \geq 2$ cut is increased by about 20%.

Since $\widetilde{W}_1\widetilde{Z}_2j$ production gives up to three leptons, we did not veto events with a third lepton to maximize the signal. Hence, we also need to include the 3-lepton background, $W\gamma^*j$. Here we include gauge bosons (W or γ^*) decaying directly to ℓ or via $\tau \to \ell\nu\nu$ chain. We see that $W\gamma^*j$ remains about a third of WWj all the way to the $N_\ell \geq 2$ cut stage.

We mention that the $(Z \to \nu\bar{\nu}) + b\bar{b} + jets$ processes – though they have cross-sections $\sim 1 - 2$ pb range after the E_T^{miss} cut – make a sub-fb contribution once we require $N_\ell \geq 2$. For this reason, we have not included these processes in the table, but have retained them in our computation of the reach in the following section.

Notice also that the single top contributions ignored in Ref. [47] are comparable to those from $\tau\bar{\tau}j$ and WWj production. The bottom line of this discussion is that the total background that we find for dilepton + monojet + E_T^{miss} events is six times larger than the value found in Ref. [47]. Moreover, as already mentioned, the bulk of our background comes from $t\bar{t}$ production in contrast to $\tau\bar{\tau}j$ production as in Han *et al.*

3.3 Enhancing the Signal: Additional Analysis Cuts

At this stage, the signal for our benchmark point with $\mu = 150$ GeV is just 2.2 fb, with a S/B ratio $\sim 0.2\%$ and a statistical significance $S/\sqrt{B} \lesssim 0.6$ even for an integrated luminosity of

1 ab^{-1}. Clearly, other analysis cuts are needed for the observability of the signal. With this in mind, we see that the signal receives contributions from $\widetilde{W}_1\widetilde{W}_1 j$, $\widetilde{Z}_1\widetilde{Z}_2 j$ and $\widetilde{Z}_2\widetilde{W}_1 j$ processes shown in Fig. 1. For the $\mu = 150$ GeV RNS point, these are 0.42 fb, 0.61 fb and 1.17 fb, respectively.[5]

The bulk of the $\tau\bar{\tau}j$ background arises from Zj events and can be efficiently removed using the kinematic procedure [63] that allows for the reconstruction of the Z-peak in di-tau events where the Z has a large transverse momentum, so that the two taus are not back-to-back in the transverse plane. Also, since the taus are ultra-relativistic, the daughter lepton and the associated neutrinos are all boosted in the direction of the parent τ momentum. In the approximation that the lepton and the neutrinos from the decay of each tau are all exactly collimated in the tau direction, we can write the momentum carried off by the two neutrinos from the decay $\tau_1 \rightarrow \ell_1 \nu\nu$ of the first tau as $\xi_1\vec{p}(\ell_1)$, and likewise for the second tau. Momentum conservation in the transverse plane requires,

$$-\vec{p}_T(j) = (1 + \xi_1)\vec{p}_T(\ell_1) + (1 + \xi_2)\vec{p}_T(\ell_2).$$

Since this is really two independent equations (recall we require $p_T(j) > 100$ GeV), it is possible to use the measured values of the jet and lepton momenta to solve these to obtain ξ_1 and ξ_2, event-by-event. It is simple to check that in the approximation of collinear tau decay, the squared mass of the di-tau system is given by

$$m_{\tau\tau}^2 = (1 + \xi_1)(1 + \xi_2)m_{\ell\ell}^2. \tag{6}$$

For dilepton plus jet events from Z-decay to taus, we expect $\xi_i > 0$ and $m_{\tau\tau}^2$ to peak at M_Z^2. Moreover, for these events, the missing energy vector will usually point in between the two lepton momentum vectors in the transverse plane. In contrast, for backgrounds where E_T^{miss} arises from neutrinos from decays of heavy SM particles (t, W, Z), the lepton and E_T^{miss} directions are uncorrelated and the E_T^{miss}-vector may point well away, or even backwards, from one of the leptons so that one (or both) $\xi_i < 0$. This is also the case for the signal where E_T^{miss} mainly arises from the undetected neutralinos. In these cases, it is entirely possible that the di-tau squared mass as given by (6) is negative.[6]

The result of our computation of $m_{\tau\tau}^2$ for dominant SM backgrounds as well as for the RNS model-line case with $\mu = 150$ GeV is illustrated in Fig. 2. The most striking feature is the relatively sharp peak at $m_{\tau\tau}^2 = M_Z^2 = 0.0083$ TeV^2 from $\tau\bar{\tau} + j$ events. The other backgrounds, as well as the signal, show a much broader distribution extending to negative values of $m_{\tau\tau}^2$ for reasons just discussed. Clearly, selecting events with

- $m_{\tau\tau}^2 < 0$

---

[5]We have checked that despite the small mass gap the leptons pass the identification requirements with an efficiency of $\sim 25\%$.

[6]Han *et al.* handle negative values of ξ_i very differently. For events with $\xi_i < 0$, they scale the corresponding neutrino energy by $-\xi_i$ so the neutrino four-vector is always time-like and $m_{\tau\tau}^2 > 0$. From our vantage point, $m_{\tau\tau}^2$ in (6) is the di-tau squared mass only for $Z \rightarrow \tau\bar{\tau}$ decays to fast taus. For all other events it is merely a kinematic quantity that facilitates the separation of this background from the signal. We do not, therefore, flip the sign of the neutrino energy when $\xi_i < 0$. We expect that our variable is a better discriminator of the signal from $Z \rightarrow \tau\bar{\tau}$ events because the procedure in Ref. [47] accidentally places some negative ξ_i events into the Z-peak.
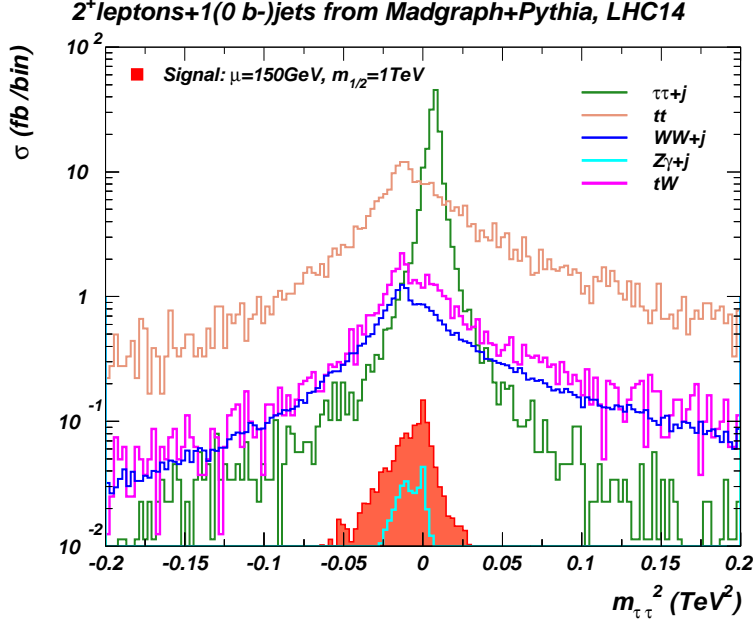
Figure 2: The distribution of $m_{\tau\tau}^2$ as defined in (6) for the main SM backgrounds to the monojet plus soft-dilepton plus E_T^{miss} signal is shown as open histograms. The shaded histogram denotes the corresponding distribution from the signal for the point on the model-line (5) with $\mu = 150$ GeV.

largely eliminates the next-to-largest $\tau\bar{\tau}j$ background (this was the largest background in Ref. [47]) and reduces other backgrounds by more than half while retaining about 60% of the signal.

As noted earlier, only about 20% of the monojet plus soft dilepton signal arises from $\widetilde{W}_1\widetilde{W}_1 j$ production. This falls to just 7% after the $m_{\tau\tau}^2 < 0$ cut just discussed. The majority of the signal thus arises from dileptons produced via leptonic decays of $\widetilde{Z}_2$ in $\widetilde{Z}_1\widetilde{Z}_2 j$ and $\widetilde{W}_1\widetilde{Z}_2 j$ events. Since lepton flavour is necessarily conserved in these decays, the signal dominantly contains same flavour (SF), opposite sign (OS) dileptons. In contrast, the background leptons for all but the tiny $Z\gamma^* j$ background in Table 1 come from the decay of two different particles, and hence are as likely to contain SF as opposite flavour (OF) leptons. This then leads us to require

- OS/SF events

in the signal. We see from the penultimate row of the Table that this halves the background with only modest loss of signal.

Before closing this discussion, we remark that background leptons originating in the decays of t, Z or W will tend to be relatively hard, so that the typical dilepton mass in these events would be $\sim M_W$. The invariant mass of the dilepton pair in signal events is bounded by $m_{\widetilde{Z}_2} - m_{\widetilde{Z}_1}$. With this in mind, we show the signal as well as background cross sections requiring, in addition,

- $m_{\ell\ell} < m_{\ell\ell}^{\mathrm{cut}}$,

where $m_{\ell\ell}^{\mathrm{cut}}$ is a cut parameter introduced in Sec. 4.1 for the optimization of the signal. For now, we fix $m_{\ell\ell}^{\mathrm{cut}} \simeq m_{\widetilde{Z}_2} - m_{\widetilde{Z}_1} \simeq 10$ GeV in the last row of Table 1. Notice that because leptons from an off-shell photon tend to be soft, the background rate from $W\gamma^* j$ becomes twice that from WWj after the $m_{\ell\ell}$ cut, even though the $W\gamma^* j$ cross-section is just a third of the WWj cross-section prior to this cut. We see that for the sample model point, we have a signal of 1.15 fb versus a background of 7.73 fb, and so would be observable with a 5σ significance with about 150 fb^{-1} of integrated luminosity.

The reader may be concerned by the fact that QCD resonances from b- and c-quarkonia may yield low mass dileptons in jetty events via their decays. While we have made no attempt to simulate this, we do not believe this will be a serious issue because the bulk of quarkonium production occurs via QCD processes, and is removed by the $E_T^{\mathrm{miss}} > 100$ GeV as well as the $N_j = 1$ requirements. Moreover, the quarkonium is very likely to be part of a jet so the daughter leptons will for the most part fail the isolation criteria.

We have also not considered detector-dependent backgrounds from non-physics processes such as jets faking electrons which would cause single-lepton plus jet processes to fake the signal. The most striking example would be Wjj production, where one of the jets is the detected hard jet, the second jet is soft, and fakes an electron, and the second lepton arises from the decay of the W. Note that since the two leptons have independent origins, the dilepton mass would typically be tens of GeV so that only a kinematically unlikely configuration could fake the signal. An estimate of this detector-dependent rate is beyond the scope of the present analysis; we only mention that the authors of Ref. [47] find this to be unimportant when the jet is from a light quark or a gluon, but find a small background from $Wb\bar{b}$ production.

4 LHC14 reach for higgsinos in the $\ell^+\ell^- j + E_T^{\mathrm{miss}}$ channel

4.1 Reach via cut-and-count experiments

We have seen that, with appropriate cuts described in the previous section, higgsino pair production in association with a hard jet leads to an observable signal in the monojet$+ E_T^{\mathrm{miss}} +$ OS/SF dilepton channel at LHC14. As seen from Table 1, the $m_{\ell\ell} < m_{\widetilde{Z}_2} - m_{\widetilde{Z}_1} \simeq 10$ GeV cut was crucial for the extraction of the signal for the $\mu = 150$ GeV test case that we had examined in the last section. However, since the neutralino mass difference is not known *a priori*, the reader may legitimately question how one would know where to set the $m_{\ell\ell}$ cut.

One possibility is to examine whether the invariant mass distribution of OS/SF dileptons exhibits an obvious mass edge from the kinematic end point of $\widetilde{Z}_2 \to \ell\bar{\ell}\widetilde{Z}_1$ after all but the $m_{\ell\ell}$ cut in Table 1. Toward this end, in Fig. 3 we show the stacked histogram of the $m_{\ell\ell}$ distribution from the various backgrounds in the table together with the 1σ error bar for just the statistical error corresponding to an integrated luminosity of 100 fb^{-1}. We include trilepton events in the histogram only if the two highest p_T leptons satisfy the OS/SF requirement. The cross-hatched histogram at low values of $m_{\ell\ell}$ shows the contribution from the higgsino signal for the model line in (5) for (*a*) $\mu = 110$ GeV, and (*b*) $\mu = 150$ GeV. As anticipated, these almost cut off at $m_{\widetilde{Z}_2} - m_{\widetilde{Z}_1}$, with the small spill-over coming mainly from leptons from $\widetilde{W}_1^+ \widetilde{W}_1^- j$ production.
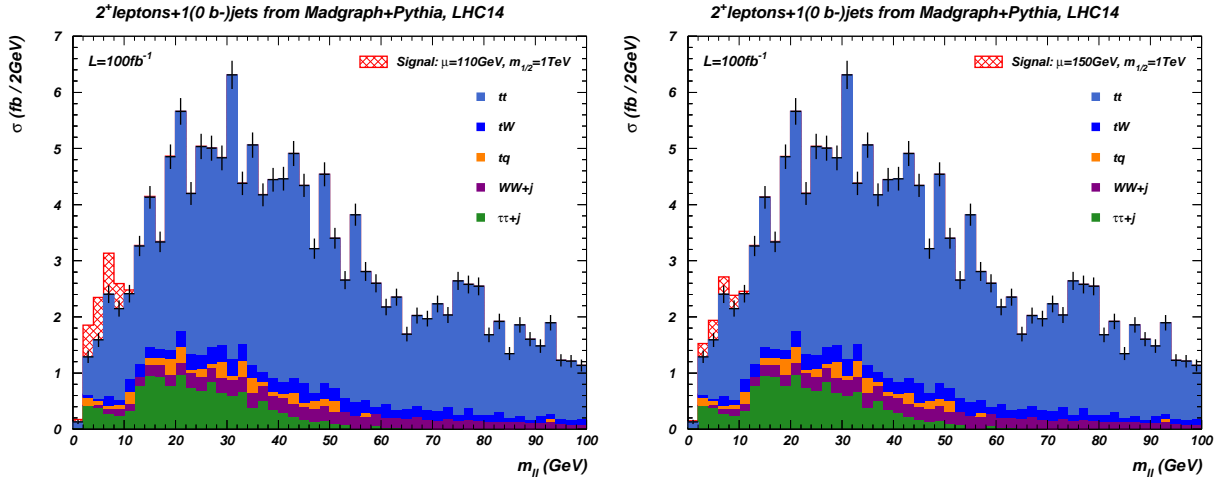
Figure 3: Stacked histogram showing various SM backgrounds listed in Table 1 of the text, together with signals for cases on the RNS model line (5) for (a) $\mu = 110$ GeV, and (b) $\mu = 150$ GeV after all the cuts in this table, except for the requirement $0 \leq m_{\ell\ell} \leq m_{\ell\ell}^{\mathrm{cut}}$ in the last row. The background histograms (solid) are stacked in the same order as the legend (the small $Z\gamma^*j$ background is not shown for clarity) while the signal is shown as the cross-hatched histogram. The error bars correspond to 1σ statistical error on the background, assuming an integrated luminosity of 100 fb^{-1}.

We note the following:

- Throughout the $m_{\ell\ell}$ range, $t\bar{t}$ production dominates other contributions to the background. Note that, for the sake of clarity, we have not included the tiny $Z\gamma^*j$ contribution on this histogram.

- Due to limited resources for computing, the $t\bar{t}$ background simulation in the figure has been performed for an integrated luminosity of just ~ 20 fb^{-1}. As a result, the bin-to-bin fluctuations in the figure are too large by a factor of $\sqrt{5}$ than would be expected in a real data sample with an integrated luminosity of 100 fb^{-1}. These fluctuations would be even smaller for still larger integrated luminosities. Ignoring these fluctuations (which are present in the figure only for technical reasons) and imagining a smoother histogram, it is clear that it should be possible to directly extract the end point of the signal for the $\mu = 110$ GeV case in frame a, though a spill-over by one bin is entirely possible. For the $\mu = 150$ GeV case in frame b, for which the signal is smaller, the location of the end point is less obvious. Most certainly, visually locating the end point of the signal would not be possible for still higher values of μ.

Rather than rely on such a visual determination of the end-point we, therefore, use the following procedure to determine the selection cut. After the cuts in all but the last row of Table 1, we require $0 \leq m_{\ell\ell} \leq m_{\ell\ell}^{\mathrm{cut}}$, where the parameter $m_{\ell\ell}^{\mathrm{cut}}$ is chosen to maximize the significance $S/\sqrt{B}$ of the signal. Since our focus here is on dileptons from $\widetilde{Z}_2$ decays for which $m_{\widetilde{Z}_2} - m_{\widetilde{Z}_1}$ is bounded from above, we begin by calculating the signal and the
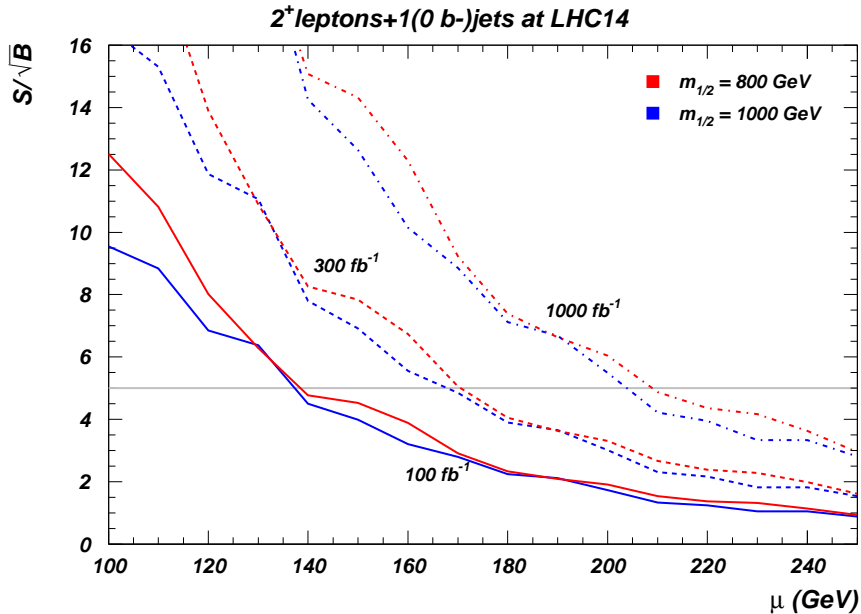
13

Figure 4: Projections for the LHC reach via monojet plus soft dileptons plus E_T^{miss} events from higgsinos versus μ, after optimization using the $m_{\ell\ell} > m_{\ell\ell}^{\mathrm{cut}}$ introduced in the text. We show results for the RNS model line of (5) (lower blue curves) and also for another model line with $m_{1/2} = 800$ GeV and the same values of other parameters (upper red curves), and for integrated luminosities of 100 fb^{-1}, 300 fb^{-1} and 1000 fb^{-1}. The grey horizontal line shows our projection for the 5σ reach neglecting any systematic uncertainty from the overall normalization of the background.

background, choosing $m_{\ell\ell}^{\mathrm{cut}}$ well beyond the end-point for the $\widetilde{Z}_2 \to \ell\bar{\ell}\widetilde{Z}_1$ decay, and evaluating the significance of the signal. As we repeat this, successively reducing the value of the cut parameter we see from Fig. 3 that at first the background reduces with the signal remaining unchanged (so that the significance increases) because $m_{\ell\ell}^{\mathrm{cut}}$ is well above the end point of the signal. However, when $m_{\ell\ell}^{\mathrm{cut}}$ goes below the kinematic end point of the signal, the signal also starts to reduce. Because the signal falls more sharply than the background a maximum of the significance is obtained. It is this value of $m_{\ell\ell}^{\mathrm{cut}}$ that maximizes the significance that we use for our projections of the LHC reach. For the analysis shown below, we used $m_{\ell\ell}^{\mathrm{cut}} = 20$ GeV to start with, and reduced it in steps of 2 GeV until we obtained the maximum significance.

We show our projections for the LHC14 reach for the RNS model line (5) – after the optimization of the $m_{\ell\ell}$ cut just described – vs. μ for integrated luminosities of 100 fb^{-1}, 300 fb^{-1} and 1000 fb^{-1} in Fig. 4. LHC14 experiments are expected to accumulate an integrated luminosity of 100 fb^{-1} (300 fb^{-1}) in a year's running at design luminosity (by the end of the run due to commence in 2015). We have also shown results extrapolated to 1 ab^{-1} integrated luminosity in anticipation of the high-luminosity (HL) LHC upgrade being considered as part of the European Strategy for Physics [64], naively assuming the same detector performance in the HL environment. For each value of integrated luminosity, we show two curves in the figure.

The lower one corresponds to $m_{1/2} = 1000$ GeV as in (5), whereas the upper one corresponds to $m_{1/2} = 800$ GeV for which the $\widetilde{Z}_2 - \widetilde{Z}_1$ mass gap ranges between 15-20 GeV (compared to ~ 10 GeV for the model line in (5)) for which the signal leptons are expected to be harder.[7] We make the following remarks:

- We see that for both cases, experiments at LHC14 will be able to discover light higgsinos via monojet plus E_T^{miss} events with identified soft dileptons in them. The reach depends on the integrated luminosity that is attained, and should extend out to $\mu \simeq 170$ GeV by the end of the next run by when an integrated luminosity of 300 fb^{-1} is anticipated, and to somewhat beyond 200 GeV at the HL LHC. While this includes the least fine-tuned parameter space of scenarios, it does not cover all models where fine-tuning is limited to 3%.

- For the $m_{1/2} = 1000$ GeV case, the optimized value of $m_{\ell\ell}^{\mathrm{cut}}$ always turns out to be 10 GeV for the entire range of the figure, whereas for the $m_{1/2} = 800$ GeV case the optimized value switches from $m_{\ell\ell}^{\mathrm{cut}} = 12$ GeV for lower values of μ to $m_{\ell\ell}^{\mathrm{cut}} = 14$ GeV for larger values in the figure.

- Although we may expect the lepton acceptance, and hence the signal, to increase for the $m_{1/2} = 800$ GeV case, we see that the LHC reach is essentially unaltered. This is because though the signal indeed does increase, the background which is rising for $m_{\ell\ell}$ values in the range of interest also increases, leaving the significance almost unaltered.

- Although our results for the reach are qualitatively similar to those of Han *et al.*, this agreement is somewhat fortuitous. The background that we find is several times larger, and the OS/SF and $m_{\ell\ell}$ cuts turn out to be crucial in our analysis.

- We note that we have been rather conservative in the criteria that we use for b-jet tagging which determine the efficiency with which b-jets can be vetoed. Recall that we assume a tagging efficiency of 60% for events with b-jets in the fiducial region. If b-jets can be more efficiently vetoed, backgrounds originating in top quarks (recall that these form the bulk of the background in Table 1) will be reduced, resulting in a correspondingly larger reach.

Before closing this section, we should mention that over the entire range of μ in Fig. 4 where the signal has a significance of more than 5σ, the signal to background ratio ranges from about 36% for low values of μ down to about 5% for $\mu > 200$ GeV and $m_{1/2} = 800$ GeV. While the distortion of the shape of the $m_{\ell\ell}$ spectrum due to the signal is evident for low values of μ, this is *not the case* for the upper end of the detectable range of μ. It is, therefore, evident that systematic errors on the *normalization of the background* will have to be controlled at considerably better than the 5% level in order to be able to claim detection of new physics. We anticipate that this will likely be feasible by direct measurements of the largest backgrounds –

---

[7]We have checked that for the $m_{1/2} = 800$ GeV model line $m_{\widetilde{Z}_2} - m_{\widetilde{W}_1}$ ranges between 4 GeV ($\mu = 100$ GeV) and about 1 GeV ($\mu = 250$ GeV). We note that the precise value of the $\widetilde{W}_1 - \widetilde{Z}_1$ mass gap is relatively unimportant because the bulk of the signal – after the OS/SF and $m_{\ell\ell}$ cuts – arises from $\widetilde{Z}_2 \rightarrow \ell\bar{\ell}\widetilde{Z}_1$ decays.

$t\bar{t}$ and $\tau\bar{\tau}j$ production – in control regions, and their extrapolation to the signal region.[8] The residual systematic using this procedure will, of course, reduce the reach from that shown in Fig. 4.

4.2   Reach via lepton flavour asymmetry

We have just seen that monojet events with soft dileptons lead to a potentially observable signal above large SM backgrounds from $t\bar{t}$, $\tau\bar{\tau}j$, di-boson plus jet and single top production. It is evident though that while the signal dileptons mostly have the same flavour e^+e^- and $\mu^+\mu^-$, each of the backgrounds listed above include an equal number of SF and OF lepton pairs. Indeed, within the SM, the expectation of $n_{\rm SM} \equiv N_{\rm SM}(SF) - N_{\rm SM}(OF)$ would be zero, but for the tiny contribution from the $Z\gamma^*j$ background in Table 1. Since $n_{\rm sig} \gtrsim n_{\rm SM}$, one might naively suppose that the difference between total rates $n \equiv N(SF) - N(OF)$ would be a good observable to discriminate the SUSY signal from SM background.

The dilepton flavour asymmetry,

$$\mathcal{A}_{\mathcal{F}} = \frac{n}{N(SF) + N(OF)} \tag{7}$$

has an added advantage that it is relatively insensitivity to the overall normalization of the background, and so does not suffer from the systematic uncertainty mentioned at the end of the previous section. The flavour asymmetry has a statistical uncertainty $\delta\mathcal{A}_{\mathcal{F}} = 1/\sqrt{N(SF) + N(OF)}$, so that the statistical significance of the flavour asymmetry signal is given by,

$$\frac{\mathcal{A}_{\mathcal{F}}}{\delta\mathcal{A}_{\mathcal{F}}} = \frac{n}{\sqrt{N(SF) + N(OF)}} \ . \tag{8}$$

Here, $N(SF)$ and $N(OF)$ are the number of same flavour and opposite flavour dilepton + jets $+E_T^{\rm miss}$ events in the sample after all cuts are applied. Neglecting the small number of dilepton events from the SUSY signal in the denominator, we see that the significance in (8) is *smaller* than the significance of the corresponding cut-and-count experiment detailed in Sec. 4.1 by a factor of about $\sqrt{2}$. We nevertheless feel that the flavour asymmetry is worthy of study as it is free of the systematic from the overall normalization of the background.

In Fig. 5 we show the flavour asymmetry $\mathcal{A}_{\mathcal{F}}$ after all cuts other than the OS/SF requirement in Fig. 3, as a function of $m_{\ell\ell}^{\rm cut}$. We show results for the SM (lower curve), and for the SUSY signal plus background (upper curve) for the RNS model-line (5) case with $\mu = 150$ GeV. Also shown are statistical error bars corresponding to an integrated luminosity of 300 fb^{-1}. In the SM the asymmetry arises dominantly from $Z(\to \nu\nu)\gamma^*j$ events which have a very small cross-section as seen in Table 1. The rate for these events peaks at small values of $m_{\ell\ell}$ because of the photon pole. All other backgrounds lead to OF and SF events at equal rates (and so no flavour asymmetry), and mostly yield dileptons with large invariant masses, causing the asymmetry to drop with increasing value of $m_{\ell\ell}^{\rm cut}$. We see though that the SM asymmetry is always smaller

---

[8]It should be possible to extrapolate the precisely measured $t\bar{t}$ cross sections in the inclusive 1 and 2 lepton channels with hard leptons to the soft dilepton channel with just one identified jet. Also the measurement of $Z(\to \ell^+\ell^-) + j$ cross sections should be straightforward to translate to the $Z(\to \tau\bar{\tau}) + j$ rates, and together with the known decay properties of τ, to the soft-lepton plus monojet signal of interest.
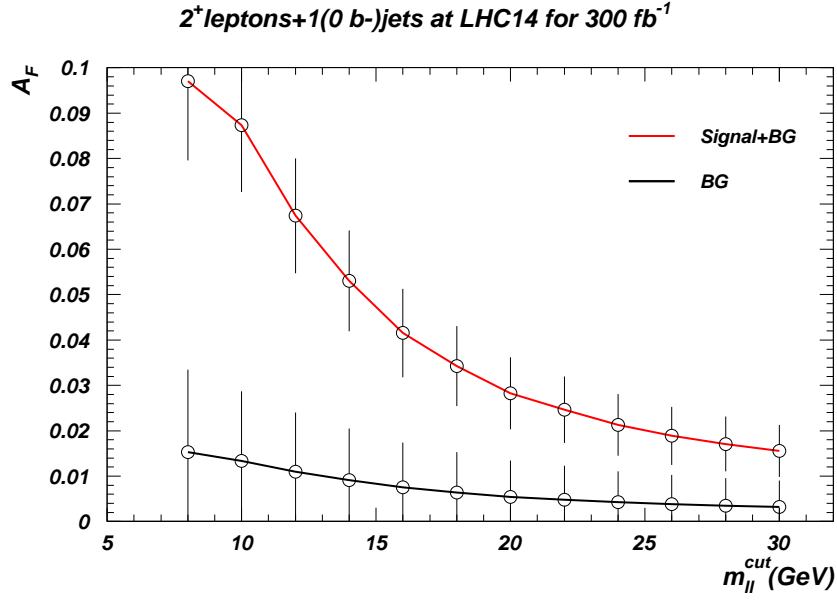
Figure 5: The flavour asymmetry $\mathcal{A}_\mathcal{F}$ introduced in (7) as a function of the cut parameter $m_{\ell\ell}^{\text{cut}}$ for the SM (lower curve), and for the higgsino signal plus background for the $\mu = 150$ GeV case on the RNS model line (5) (upper curve), after the cuts in Table 1 except, of course, the OS/SF cut in the penultimate row, but with the requirement $0 < m_{\ell\ell} < m_{\ell\ell}^{\text{cut}}$. The error bars are for an integrated luminosity of 300 fb^{-1} at LHC14.

than 1.5% for $m_{\ell\ell}^{\text{cut}} > 8$ GeV. The flavour asymmetry from the higgsino production arises via dileptons from $\widetilde{Z}_2 \to \widetilde{Z}_1 \ell\bar{\ell}$ decay and is also diluted if $m_{\ell\ell}^{\text{cut}} > m_{\widetilde{Z}_2} - m_{\widetilde{Z}_1}$. Since the rate for the signal substantially exceeds that for the $Z\gamma^* j$ background, the asymmetry expected is significantly larger than in the SM. Indeed, we see from Fig. 5 that with a judicious choice of $m_{\ell\ell}^{\text{cut}}$, LHC14 experiments – with an integrated luminosity of 300 fb^{-1} – should be able to distinguish the flavour asymmetry produced via higgsinos from that in the SM at about the 5σ level.

To obtain the optimal value of $m_{\ell\ell}^{\text{cut}}$, we follow the procedure used in Fig. 4: *i.e.* we choose $m_{\ell\ell}^{\text{cut}}$ that maximizes the statistical significance $\mathcal{A}_\mathcal{F}/\delta\mathcal{A}_\mathcal{F}$. Our projection for the LHC14 reach via the flavour asymmetry determination is shown in Fig. 6. We see that LHC14 experiments will be able to discover higgsinos at 5σ for μ values up to ~ 120 GeV, ~ 160 GeV and ~ 205 GeV for integrated luminosities of 100 fb^{-1}, 300 fb^{-1} and 1000 fb^{-1}, respectively. These projections are 10-15 GeV smaller than the corresponding reach shown in Fig, 4 because of the additional factor of $\sim \sqrt{2}$ in the statistical significance $\mathcal{A}_\mathcal{F}/\delta\mathcal{A}_\mathcal{F}$ as discussed just below Eq. (8). We remind the reader that the result in Fig. 6 will, however, not be sensitive to the systematic uncertainty from the normalization of the background which would, of course, reduce the corresponding reach in Fig. 4.
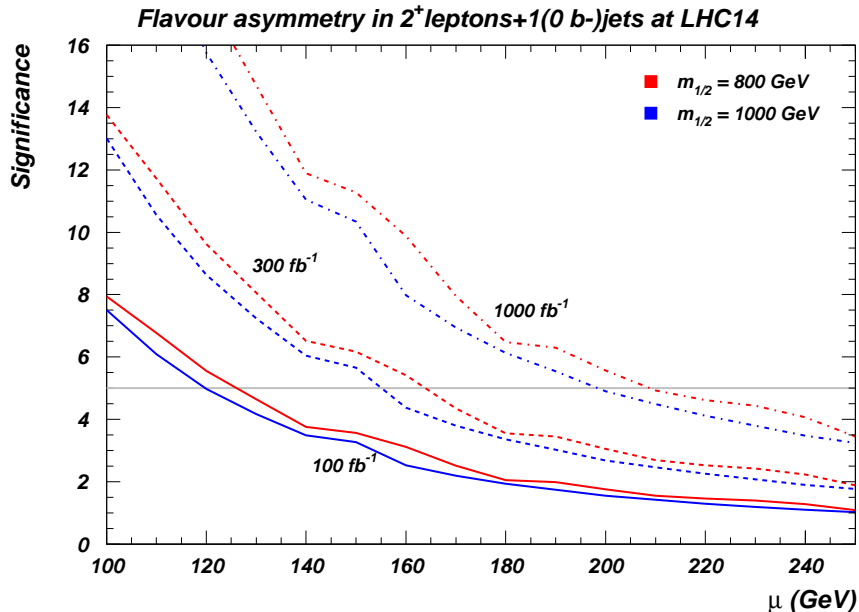
Figure 6: Our projections for the LHC14 reach for higgsinos via measurements of flavour asymmetry as a function of μ after optimization using the $m_{\ell\ell} > m_{\ell\ell}^{\text{cut}}$ introduced in the text. We show results for the same two model lines as in Fig. 4 for integrated luminosities of 100 fb^{-1}, 300 fb^{-1} and 1000 fb^{-1}.

5   Concluding remarks

The most conservative expression of naturalness as embodied in Eq. (1) requires that the weak scale value of the higgsino mass μ be not to far from the measured value of M_Z. Because high scale gaugino mass parameters can be as large as ~ 2 TeV without jeopardizing naturalness, the existence of four light higgsino-like electroweak -inos with compressed spectra is a robust feature of natural SUSY.

While natural SUSY may be discovered at LHC14 via gluino pair production [48] or same-sign diboson production [65, 48], the reach in these channels (assuming gaugino mass unification) is restricted to $m_{\tilde{g}} \lesssim 2$ TeV (depending on assumed integrated luminosity). Meanwhile, direct pair production of higgsinos can occur with cross sections in the 10-100 fb range. However, these are difficult to detect because the energy release from higgsino decays is typically very small. In models with gaugino mass unification, the mass gap between the second lightest and the lightest (higgsino-like) neutralinos can be as small as 10 GeV if Δ_{EW}^{-1} is limited to 3%. As a result, higgsino pair production at the LHC (even if it could somehow be triggered on) would be buried under large SM.

This led several groups to examine the possibility of detecting higgsino pair production events produced in association with a central, hard jet from QCD radiation. While there is indeed an observable event rate for these "monojet events" (monojet, because the decay products of heavier higgsinos are very soft), this strategy suffers from the fact that the signal,

which is typically just 1% of the background, does not have any kinematic features that help to distinguish it from $Z(\to \nu\nu) + j$ production in the SM. The normalization of the background would, therefore, have to be known at considerably better than the percent level to be able to claim a signal, a daunting prospect for tails of backgrounds of QCD origin.

Giudice *et al.* [31] suggested that it may be possible to reduce the background by requiring additional soft leptons in these monojet events. Following this lead, Han *et al.* [47] concluded that with the additional requirement of two soft leptons, LHC experiments should be sensitive to the higgsino signal above SM backgrounds from $(Z \to \tau\tau) + j$ production, from $t\bar{t}$ production and from WWj production even if the neutralino mass gap is relatively small. Prior to this study, it was widely believed that the ILC was essential for the discovery of light higgsinos of natural SUSY if the mass gap is small.

The importance of the LHC discovery potential for light higgsinos led us to revisit the issue in this paper. We used the RNS framework (outlined in Sec. 2) that we have previously developed for phenomenological analyses of natural SUSY to guide our thinking. For our analysis, we re-evaluated the backgrounds listed by Han *et al.* along with several other significant background sources: see Table 1. With similar cuts, the total background that we find is about 25 times that in Ref. [47]. We have described our attempt to track down the causes of the difference in Sec. 3. In light of this order-of-magnitude larger background, we were led to more detailed cuts, including the OS/SF and $m_{\ell\ell}$ requirements for the signal dileptons in order to extract the signal. Remarkably, after a lengthy analysis, we find a higgsino reach, as measured by the reach in $|\mu|$, qualitatively similar to that in Ref. [47]. With an integrated luminosity of 300 fb^{-1} – targeted for accumulation before the shutdown for the high luminosity upgrade of the LHC – experiments should be sensitive to higgsinos at the 5σ level if $|\mu| < 170$ GeV, while the high luminosity upgrades should be sensitive to μ values as high as 210 GeV: see Fig. 4.[9] It should be emphasized that the sensitivity in this figure is evaluated using just the expected statistical error in the background which is assumed to be measured or calculated, and does not include any error from the uncertainty of the background. Inclusion of this systematic uncertainty will reduce the signal significance, and hence the reach. This could be relevant especially at the high-luminosity upgrade where the signal to background ratio for $\mu \sim 200$ GeV is just 5%.

In addition to projecting the LHC14 reach of higgsinos from a traditional cut-and-count experiment, we have also evaluated the LHC reach obtained via the measurement of the flavour asymmetry variable introduced in Eq. (7). We see from Fig. 6 that the LHC reach for μ via this measurement is just 10-15 GeV smaller than that in Fig. 4. This procedure, however, has the important advantage that this reach is insensitive to systematic uncertainties from the background normalization. We also see from Fig. 6 that, in contrast to the reach from the counting experiment in Fig. 4, the reach via the flavour asymmetry measurement increases with increasing neutralino mass gap.

We cannot overstress the importance of the direct search for higgsinos as these could well be the only accessible superpartners at LHC14. Gluinos and first generation squarks may be in the multi-TeV range without jeopardizing naturalness. Top squarks may also be in

---

[9]We reiterate that, since top pair production is by far the dominant background in Table 1, our projections for the reach are sensitive to our assumptions about how well we can veto b-jets. Here, we have conservatively assumed a tagging efficiency of just 60% for b-jets in the fiducial region, for the upcoming LHC run, as well as for the high luminosity upgrade of the LHC.

the 1-2 TeV range, well beyond the LHC reach. Signals from wino production that could lead to characteristic same-sign dilepton events without hard jet activity [65] may well be accessible at the high luminosity upgrade of the LHC even if gluinos are inaccessible. But again, the accessibility of winos at even the high luminosity LHC is not guaranteed by naturalness considerations.

In summary, LHC14 will be sensitive to light higgsinos of natural SUSY models via the search for monojet events with identified OS/SF dileptons, mostly from the decays $\widetilde{Z}_2 \to \widetilde{Z}_1 \ell\bar{\ell}$. These dileptons necessarily have low invariant masses, $m_{\ell\ell} < m_{\widetilde{Z}_2} - m_{\widetilde{Z}_1}$. Even with an integrated luminosity of 100 fb^{-1} expected from a year of LHC operation at the design luminosity, the sensitivity of LHC14 experiments to higgsinos should reach beyond what was explored at LEP200, and up to about what may be observable at ILC250 [29]. The LHC reach grows with integrated luminosity, but even with ~ 1 ab^{-1} of integrated luminosity, the reach in μ extends to just over 200 GeV. While the LHC can indeed probe models of SUSY with the smallest fine-tuning, it appears that an electron-positron linear collider with $\sqrt{s} = 600$ GeV is essential for a complete exploration of natural SUSY models with less than 3% electroweak fine-tuning. It is, nonetheless, exciting that LHC14 could be a discovery machine for higgsinos of natural SUSY.

Acknowledgments

References

[1] G. Aad *et al.* [ATLAS Collaboration], *Phys. Rev.* **D 87** (2013) 012008, *J. High Energy Phys.* **1409** (2013) 176, *J. High Energy Phys.* **1410** (2014) 24 and ATLAS-CONF-2013-062.

[2] S. Chatrchyan *et al.* [CMS Collaboration], *J. High Energy Phys.* **1210** (2012) 018 and CMS-PAS-SUS-13-019.

[3] G. Aad *et al.* [ATLAS Collaboration], *Phys. Lett.* **B 716** (2012) 1.

[4] S. Chatrchyan *et al.* [CMS Collaboration], *Phys. Lett.* **B 716** (2012) 30.

[5] H. Baer, V. Barger and D. Mickelson, *Phys. Rev.* **D 88** (2013) 095013.

[6] H. Baer, V. Barger, D. Mickelson and M. Padeffke-Kirkland, *Phys. Rev.* **D 89** (2014) 115019.

[7] See, *e.g.* H. Baer and X. Tata, *Weak Scale Supersymmetry: From Superfields to Scattering Events*, (Cambridge University Press, 2006).

[8] H. Baer, V. Barger, P. Huang, D. Mickelson, A. Mustafayev and X. Tata, *Phys. Rev.* **D 87** (2013) 115028.

[9] H. Baer, V. Barger, P. Huang, A. Mustafayev and X. Tata, *Phys. Rev. Lett.* **109** (2012) 161802.

[10] M. Perelstein and C. Spethmann, *J. High Energy Phys.* **0704** (2007) 070, also considered a fine-tuning measure defined in terms of weak scale parameters.

[11] K. Chan, U. Chattopadhyay and P. Nath, *Phys. Rev.* **D 58** (1998) 096004.

[12] H. Baer, V. Barger, P. Huang, D. Mickelson, A. Mustafayev and X. Tata, *Phys. Rev.* **D 87** (2012) 035017.

[13] R. Kitano and Y. Nomura, *Phys. Lett.* **B 631** (2005) 58, *Phys. Rev.* **D 73** (2006) 095004 and hep-ph/0606134.

[14] M. Papucci, J. T. Ruderman and A. Weiler, *J. High Energy Phys.* **1209** (2012) 035.

[15] J. Ellis, K. Enqvist, D. Nanopoulos and F. Zwirner, Mod. Phys. Lett. **A1** (1986) 57.

[16] R. Barbieri and G. Guidice, *Nucl. Phys.* **B 306** (1988) 36.

[17] A. Mustafayev and X. Tata, Indian J. Phys. **88**, 991 (2014) [arXiv:1404.1386 [hep-ph]].

[18] J. Casas, J. Moreno, S. Robies and K. Rolbiecki, arXiv:1407.6966 [hep-ph].

[19] J. Feng, K. Matchev and T. Moroi, *Phys. Rev.* **D 61** (2000) 075005.

[20] J. Feng, K. Matchev and D. Sanford, *Phys. Rev.* **D 85** (2012) 075007 [arXiv:1112.3021 [hep-ph]]; J. Feng and D. Sanford, *Phys. Rev.* **D 86** (2012) 055012 [arXiv:1205.2372 [hep-ph]].

[21] H. Baer, A. Mustafayev, S. Profumo, A. Belyaev and X. Tata, *Phys. Rev.* **D 71** (2005) 095008.

[22] D. Matalliotakis and H. P. Nilles, *Nucl. Phys.* **B 435** (1995) 115; V. Berezinski *et al. Astropart. Phys.* **5** (1996) 333; P. Nath and R. Arnowitt, *Phys. Rev.* **D 56** (1997) 2820; A. Bottino, F. Donato, N. Fornengo and S. Scopel, *Phys. Rev.* **D 59** (1999) 095004 and *Phys. Rev.* **D 63** (2001) 125003; J. Ellis, K. Olive and Y. Santoso, *Phys. Lett.* **B 539** (2002) 107; J. Ellis, T. Falk, K. Olive and Y. Santoso, *Nucl. Phys.* **B 652** (2003) 259; H. Baer, A. Mustafayev, S. Profumo, A. Belyaev and X. Tata, *J. High Energy Phys.* **0507** (2005) 065; See T. Li and S. Raza, arXiv:1409.3930 [hep-ph] for a recent study.

[23] H. Baer, A. Mustafayev, H. Summy and X. Tata, *J. High Energy Phys.* **0710** (2007) 088 [arXiv:0708.4003 [hep-ph]].

[24] U. Chattopadhyay and D. P. Roy, *Phys. Rev.* **D 68** (2003) 033010 [hep-ph/0304108]; H. Baer, A. Mustafayev, E-K. Park, S. Profumo and X. Tata, *J. High Energy Phys.* **0604** (2006) 041 [hep-ph/0603197]; S. P. Martin, *Phys. Rev.* **D 75** (2007) 115005 [hep-ph/0703097]; I. Gogoladze, F. Nasir and Q. Shafi, Int. J. Mod. Phys. A **28** (2013) 1350046; I. Gogoladze, F. Nasir and Q. Shafi, *J. High Energy Phys.* **1311** (2013) 173.

[25] J. E. Younkin and S. P. Martin, *Phys. Rev.* **D 85** (2012) 055028; S. Martin, *Phys. Rev.* **D 89** (2014) 035011.

[26] For a review, see U. Ellwanger, C. Hugonie and A. M. Teixeira, Phys. Rept. **496**, 1 (2010) [arXiv:0910.1785 [hep-ph]].

[27] G. Giudice and A. Masiero, *Phys. Lett.* **B 206** (1988) 480.

[28] J. E. Kim and H. P. Nilles *Phys. Lett.* **B 138** (1984) 150.

[29] H. Baer, V. Barger, D. Mickelson, A. Mustafayev and X. Tata, *J. High Energy Phys.* **1406** (2014) 172 [arXiv:1404.7510 [hep-ph]].

[30] M. Berggren, F. Brümmer, J. List, G. Moortgat-Pick, T. Robens, K. Rolbiecki and H. Sert, *Eur. Phys. J.* **C 73** (2013) 2660.

[31] G. F. Giudice, T. Han, K. Wang and L. T. Wang, *Phys. Rev.* **D 81** (2010) 115011 [arXiv:1004.4902 [hep-ph]].

[32] H. Baer, V. Barger and P. Huang, *J. High Energy Phys.* **1111** (2011) 031 [arXiv:1107.5581 [hep-ph]].

[33] H. Zhang, Q. Cao, C. Chen and C. Li, *J. High Energy Phys.* **1108** (2011) 018; M. Beltran, D. Hooper, E. W. Kolb, Z. A. C. Krusberg and T. M. P. Tait, *J. High Energy Phys.* **1009** (2010) 037 [arXiv:1002.4137 [hep-ph]]; J. Goodman, M. Ibe, A. Rajaraman, W. Shepherd, T. M. P. Tait and H. B. Yu, *Phys. Rev.* **D 82** (2010) 116010 [arXiv:1008.1783 [hep-ph]]; A. Rajaraman, W. Shepherd, T. M. P. Tait and A. M. Wijangco, *Phys. Rev.* **D 84** (2011) 095013 [arXiv:1108.1196 [hep-ph]].

[34] P. J. Fox, R. Harnik, J. Kopp and Y. Tsai, *Phys. Rev.* **D 85** (2012) 056011 [arXiv:1109.4398 [hep-ph]].

[35] C. Han, A. Kobakhidze, N. Liu, A. Saavedra, L. Wu and J. M. Yang, *J. High Energy Phys.* **1402** (2014) 049 [arXiv:1310.4274 [hep-ph]].

[36] H. Baer, A. Mustafayev and X. Tata, *Phys. Rev.* **D 89** (2014) 055007 [arXiv:1401.1162 [hep-ph]].

[37] P. Schwaller and J. Zurita, *J. High Energy Phys.* **1403** (2014) 060 [arXiv:1312.7350 [hep-ph]].

[38] G. Aad *et al.* [ATLAS Collaboration], *J. High Energy Phys.* **1304** (2013) 075 [arXiv:1210.4491 [hep-ex]]; S. Chatrchyan *et al.* [CMS Collaboration], *J. High Energy Phys.* **1209** (2012) 094 [arXiv:1206.5663 [hep-ex]]; V. Khachatryan *et al.* [CMS Collaboration], arXiv:1408.3583 [hep-ex].

[39] A. Anandkrishnan, L. Carpenter and S. Raby, *Phys. Rev.* **D 90** (2014) 055004.

[40] G. Aad *et al.* [ATLAS Collaboration], *Phys. Rev. Lett.* **110** (2013) 011802.

[41] S. Chatrchyan *et al.* [CMS Collaboration], *Phys. Rev. Lett.* **108** (2012) 261803 [arXiv:1204.0821 [hep-ex]].

[42] J. Bramante, A. Delgado, F. Elahi, A. Martin and B. Ostdiek, arXiv:1408.6530 [hep-ph].

[43] N. F. Bell, J. B. Dent, A. J. Galea, T. D. Jacques, L. M. Krauss and T. J. Weiler, *Phys. Rev.* **D 86** (2012) 096011 [arXiv:1209.0231 [hep-ph]]; L. M. Carpenter, A. Nelson, C. Shimmin, T. M. P. Tait and D. Whiteson, *Phys. Rev.* **D 87** (2013) no. 7, 074005 [arXiv:1212.3352]; A. Anandakrishnan, L. M. Carpenter and S. Raby, *Phys. Rev.* **D 90** (2014) 055004.

[44] G. Aad *et al.* [ATLAS Collaboration], *Phys. Rev.* **D 90** (2014) 012004 [arXiv:1404.0051 [hep-ex]], *Phys. Rev. Lett.* **112** (2014) no. 4, 041802 [arXiv:1309.4017 [hep-ex]] and arXiv:1407.7494 [hep-ex]; V. Khachatryan *et al.* [CMS Collaboration], arXiv:1408.2745 [hep-ex].

[45] A. A. Petrov and W. Shepherd, *Phys. Lett.* **B 730** (2014) 178 [arXiv:1311.1511 [hep-ph]]; L. Carpenter, A. DiFranzo, M. Mulhearn, C. Shimmin, S. Tulin and D. Whiteson, *Phys. Rev.* **D 89** (2014) 075017 [arXiv:1312.2592 [hep-ph]]; A. Berlin, T. Lin and L-T. Wang, *J. High Energy Phys.* **1406** (2014) 078 [arXiv:1402.7074 [hep-ph]].

[46] O. Buchmueller, M. J. Dolan and C. McCabe, *J. High Energy Phys.* **1401** (2014) 025 [arXiv:1308.6799 [hep-ph]].

[47] Z. Han, G. D. Kribs, A. Martin and A. Menon, *Phys. Rev.* **D 89** (2014) 075007 [arXiv:1401.1235 [hep-ph]].

[48] H. Baer, V. Barger, P. Huang, D. Mickelson, A. Mustafayev, W. Sreethawong and X. Tata, *J. High Energy Phys.* **1312** (2013) 013 [arXiv:1310.4858 [hep-ph]].

[49] H. Baer, V. Barger, M. Padeffke-Kirkland and X. Tata, *Phys. Rev.* **D 89** (2014) 037701 [arXiv:1311.4587 [hep-ph]].

[50] M. Dine, A. Kagan and S. Samuel, *Phys. Lett.* **B 243** (1990) 250; A. Cohen, D. B. Kaplan and A. Nelson, *Phys. Lett.* **B 388** (1996) 588; J. Bagger, J. Feng and N. Polonsky, *Nucl. Phys.* **B 563** (1999) 3.

[51] See H. Murayama and A. Pierce, *Phys. Rev.* **D 65** (2002) 055009, for a discussion of issues with the proton life-time.

[52] S. Weinberg, *Phys. Rev. Lett.* **48** (1982) 1303; M. Khlopov and A. Linde, *Phys. Lett.* **B 138** (1984) 265; M. Kawasaki, A. Kohri, T. Moroi and A. Yotsuyanagi, *Phys. Rev.* **D 78** (2008) 065011.

[53] ISAJET, by H. Baer, F. Paige, S. Protopopescu and X. Tata, hep-ph/0312045.

[54] J. Alwall, M. Herquet, F. Maltoni, O. Mattelaer and T. Stelzer, *J. High Energy Phys.* **1106** (2011) 128.

[55] M. Mangano, M. Moretti, F. Piccinini and M. Treccani, *J. High Energy Phys.* **0701** (2007) 013.

[56] T. Sjostrand, S. Mrenna. P. Z. Skands, *J. High Energy Phys.* **0605** (2006) 026.

[57] CTEQ Collaboration, J. Botts *et al. Phys. Lett.* **B 04** (1993) 1959, and J. Pumplin, D. R. Stump, J. Huston, H. L. Lai, P. M. Nadolsky and W. K. Tung, *J. High Energy Phys.* **0207** (2002) 012 [hep-ph/0201195].

[58] S. Jadach, J. H. Kuhn and Z. Was, Comput. Phys. Commun. **64**, 275 (1990); O. Shekhovtsova, I. M. Nugent, T. Przedzinski, P. Roig and Z. Was, AIP Conf. Proc. **1492**, 62 (2012) [arXiv:1208.5420 [hep-ph]].

[59] T. Stelzer, Z. Sullivan and S. Willenbrock, *Phys. Rev.* **D 56** (1997) 5919 [hep-ph/9705398] and *Phys. Rev.* **D 58** (1998) 094021 [hep-ph/9807340]; A. S. Belyaev, E. E. Boos and L. V. Dudko, *Phys. Rev.* **D 59** (1999) 075001 [hep-ph/9806332].

[60] M. Czakon, P. Fiedler and A. Mitov, *Phys. Rev. Lett.* **110** (2013) no. 25, 252004 [arXiv:1303.6254 [hep-ph]].

[61] G. Cullen, N. Greiner and G. Heinrich, *Eur. Phys. J.* **C 73** (2013) 2388 [arXiv:1212.5154 [hep-ph]].

[62] PROSPINO program: W. Beenakker, M. Klasen, M. Kramer, T. Plehn, M. Spira and P. M. Zerwas, *Phys. Rev. Lett.* **83** (1999) 3780 [Erratum-ibid. **100**, 029901 (2008)] [hep-ph/9906298].

[63] R. K. Ellis, I. Hinchliffe, M. Soldate and J. J. van der Bij, *Nucl. Phys.* **B 297** (1988) 221.

[64] T. Akesson, R. Aleksan, B. Allanach, S. Bertolucci, A. Blondel, J. Butterworth, M. Cavalli-Sforza and A. Cervera *et al.*, *Eur. Phys. J.* **C 51** (2007) 421 [hep-ph/0609216]; ATLAS-Collaboration, "Physics at a High-Luminosity LHC with ATLAS," ATL-PHYS-PUB-2012-001; ATLAS-collaboration, "Physics at a High-Luminosity LHC with ATLAS (Update)," ATL-PHYS-PUB-2012-004; S. Rajagopalan [ATLAS Collaboration], EPJ Web Conf. **49** (2013) 11004; CMS Collaboration, CMS-Note 2012/006.

[65] H. Baer, V. Barger, P. Huang, D. Mickelson, A. Mustafayev, W. Sreethawong and X. Tata, *Phys. Rev. Lett.* **110** (2013) 151801.